

## EXPERIMENTAL ANALYSIS OF PARTITION COEFFICIENT IN Al-Mg ALLOYS

M. H. Avazkonandeh-Gharavol<sup>1</sup>, M. Haddad-Sabzevar<sup>\*2</sup> and H. Fredriksson<sup>3</sup>

\* haddadm@um.ac.ir

Received: March 2015

Accepted: October 2015

<sup>1</sup> Department of Materials and Polymer Engineering, Faculty of Engineering, Hakim Sabzevari University, Sabzevar, Iran.

<sup>2</sup> Department of Metallurgical and Materials Engineering, Faculty of Engineering, Ferdowsi University of Mashhad, Mashhad, Iran.

<sup>3</sup> Department of Materials Science and Engineering, Royal Institute of Technology (KTH), Brinellvägen 23, 100 44 Stockholm, Sweden.

**Abstract:** Because the partition coefficient is one of the most important parameters affecting microsegregation, the aim of this research is to experimentally analyse the partition coefficient in Al-Mg alloys. In order to experimentally measure the partition coefficient, a series of quenching experiments during solidification were carried out. For this purpose binary Al-Mg alloys containing 6.7 and 10.2 wt-% Mg were melted and solidified in a DTA furnace capable of quenching samples during solidification. Cooling rates of 0.5 and 5 K/min were used and samples were quenched from predetermined temperatures during solidification. The fractions and compositions of the phases were measured by quantitative metallography and SEM/EDX analyses, respectively. These results were used to measure the experimental partition coefficients. The resultant partition coefficients were used to model the concentration profile in the primary phase and the results were compared with equilibrium calculations and experimental profiles. The results of calculations based on the experimental partition coefficients show better consistency with experimental concentration profiles than the equilibrium calculations.

**Keywords:** Partition Coefficient, Microsegregation, Al-Mg Alloys, Differential Thermal Analysis.

### 1. INTRODUCTION

Thermal analysis is an efficient method to study the solidification of metals and alloys [1]. Controlling solidification process is very important and understanding the solidification curves, i.e. the solidification sequences and solid fraction versus temperature during solidification are crucial for the control of solidification processes [2]. The liquid fraction can affect alloy castability and formability. In particular, the last 10% fractional evolution during casting significantly affects casting defects such as hot tearing and porosity [3]. The direct measurement of the fractional change as a function of temperature is difficult. The amount of liquid is usually estimated either by quantitative image analysis of quenched samples or by using enthalpy measurements [2].

Aluminium alloys are frequently used in automobile and aerospace industries to reduce the weight of components and structures. Al-Mg alloys are one of the major Al alloys groups

which widely used because of their special features such as high resistance to corrosion, good machinability and attractive appearance when anodized. The magnesium contents of the binary alloys range from 4 to 10% [4]. Casting processes are the most important methods in the manufacturing of aluminium alloys [4]. The solidification behaviour of the ingot has a great influence on the mechanical and physical properties of cast Al alloys. Microsegregation, which is non-uniform distribution of alloying elements in the scale of secondary dendrite arm spacing, is one of the most important phenomena occurring during solidification. It usually results in formation of some unexpected second phases which generally reduce the workability of casting products. Because of its industrial importance, this subject has been extensively studied during the last decades both theoretically and experimentally and there are several models which can predict the microsegregation with different degrees of accuracy [5-9].

The main reason for formation of

microsegregation is thermodynamics of solidification and hence partition coefficient ( $k_0$ ) [10]. It is defined by equation (1) [11].

$$k_0 = \frac{C_S^i}{C_L^i} \quad (1)$$

where  $C_S^i$  and  $C_L^i$  are concentrations of solute atoms in solid and liquid at the solid/liquid interface, respectively. In most cases  $k_0 < 1$ , and during solidification the alloying elements prefer to remain in the liquid.

Different mechanisms which affect microsegregation are back diffusion, coarsening, and undercooling [7]. In recent years some of the researchers have noticed that the inconsistency between experimental and calculated results may come from the inaccurate data used in models, such as diffusion and/or partition coefficients. Chang [12,13] and Hunt [14] and their colleagues tried to generate some new data on phase diagram and diffusion coefficient and used them to model the microsegregation in Al-Cu alloys. They showed that with these new data better correlation with experimental results can be achieved [12-14].

The study of microsegregation can be divided in three parts: physical basis, modelling process, and data used in the modelling. The first two parts have been deeply studied in the literature. But the data which are usually used in modelling are from very old references (which might not be accurate enough) and so they can cause some errors in calculations. Most of the thermodynamic data, such as  $k_0$  which is extracted from phase diagram, is applicable for equilibrium conditions and is not appropriate for practical (or non-equilibrium) situations. Most of the previous researches on microsegregation focus mainly on Al-Cu alloys [1-3,12-15]. Al-Mg system is also one of the major alloying systems in aluminium alloys, but did not deeply investigated in the literature [15,16]. So, the aim of this paper is to experimentally measure the  $k_0$  for binary Al-Mg alloys. The experimental and equilibrium partition coefficients were used to calculate the concentration profiles across the

secondary dendrite arms. The calculated profiles were compared to experimental profiles and the origin of discrepancies is discussed.

## 2. EXPERIMENTAL PROCEDURE

High purity binary Al-Mg alloys were prepared as model alloys. The chemical compositions of the alloys were determined by optical emission spectrometry (OES). The alloys contain 6.7 and 10.2 wt-% Mg and about 0.06 wt-% Fe and 0.05 wt-% Si were also detected which are negligible.

For thermal analysis a Mettler DTA furnace capable of quenching samples during solidification was used. For this purpose about 1 g of the alloys was melted for each sample, held at 700 °C for 10 min, cooled at rates of 0.5 and 5 K/min, and quenched from predetermined temperatures during cooling. The quenching temperatures were selected according to the preliminary experiments. In each set of experiments one sample was quenched after its complete solidification. High purity argon gas (99.999%) was flown during the DTA tests to reduce the risk of oxidation. Samples coding and the values of the experimental parameters are listed in Table 1.

The microstructure of the samples which are quenched during solidification can be divided into two parts. First part contains coarse primary  $\alpha$ -Al dendrites which formed before quenching. The second part consists of very fine primary dendrites and eutectic phases which formed during quenching. The first part will be called 'primary phase' and the second part 'quenched melt' hereafter. The samples were prepared for microstructural and compositional analysis by conventional methods. Fractions of the phases were determined by manual swift point counting method based on the ASTM E562-11 standard after etching in 0.5% HF solution. In most of the quenched samples, dendrite arms can be distinguished and their spacing (SDAS) can be easily measured from the optical micrographs. For those samples which the dendrite arms could not be distinguished, because of coalescence of the dendrite arms, samples were etched with Weck's reagent.

In some of the samples, concentration profiles in primary phase were determined by Hitachi S-3700 N SEM equipped with EDX detector. The EDX detector was first calibrated with standard sample containing 4.5 wt-% Mg. In order to have statistically significant concentration profiles in the solid, around 100 points were analysed by SEM/EDX point analysis technique. These data were processed to obtain concentration profiles in the solid based on the method proposed by Gungor [17]. For the samples which the concentration profiles were not determined the minimum concentration in the primary phase ( $C_{min}$ ) was measured by around 20 SEM/EDX point analyses at nearly the center of the dendrites. In the quenched samples,  $C_L$  was measured by SEM/EDS areal analysis. At least 5 areas were analysed and their average value was used as  $C_L$ .

Partition coefficient was calculated with 4 different methods as described below. In the first method the experimentally measured  $C_L$  and fraction of quenched melt ( $f_L$ ) were inserted in

Scheil equation to estimate  $k_0$  value. In the second method, the measured  $C_L$  and  $f_L$  were used as input data in the Lever rule to calculate the  $k_0$ . In the third method, minimum concentration of Cu was measured from SEM/EDX point analyses in the primary phase and the  $k_0$  was calculated from the Equation (2).

$$k_0^{Exp} = \frac{C_{min}}{C_0} \quad (2)$$

In the fourth method, the Scheil equation was fitted to the experimental concentration profile using least square method with  $k_0$  as a free parameter [18].

### 2. 1. Modelling of Microsegregation

A numerical model which takes into account the back diffusion in the solid and diffusion in the liquid was used to model the microsegregation during solidification. As the low cooling rates were used, effects of eutectic undercooling and coarsening were ignored [19]. To calculate the concentration profiles in the solid and liquid, the Fick's second law, equations (3) and (4), were solved separately in the solid and liquid.

$$\frac{\partial C_S}{\partial t} = \frac{\partial}{\partial x} \left( D_S \frac{\partial C_S}{\partial x} \right)_{\xi} \quad (3)$$

$$\frac{\partial C_L}{\partial t} = \frac{\partial}{\partial x} \left( D_L \frac{\partial C_L}{\partial x} \right)_{\xi} \quad (4)$$

where  $C_S$ ,  $C_L$ ,  $D_S$ ,  $D_L$ ,  $\xi$  and  $d$  are concentrations in the solid and liquid, diffusion coefficients in the solid and liquid, interface position, and length of volume element (which is half of the dendrite arm spacing), respectively. The mass balance is:

$$\int_0^{\xi} (C_S \times dx_S) + \int_{\xi}^d (C_L \times dx_L) = d \times C_0 \quad (5)$$

**Table 1.** Samples coding and experimental parameters used to prepare the samples

Sample code	Mg Content (wt-%)	Cooling Rate (K/min)	Quenching Temperature (°C)
7MgS1	6.7	0.5	605
7MgS2			580
7MgS3			540
7MgSF			435
7MgM1		5	605
7MgM2			580
7MgM3			540
7MgMF			435
10MgS1	10.2	0.5	580
10MgS2			540
10MgS3			500
10MgSF			435
10MgM1		5	580
10MgM2			540
10MgM3			500
10MgMF			435

Additional mass balance is also needed at the interface [20] as following:

$$\left( D_s \frac{\partial C_s}{\partial x} \right) - \left( D_L \frac{\partial C_L}{\partial x} \right) = (C_L - C_s) \frac{d\xi}{dt} \quad (6)$$

The above equations were solved according to the numerical scheme proposed by Tanzili and Heckel [21]. For this purpose a volume element, as shown in Fig. 1, was considered and divided into  $N$  nodes:  $r$  nodes in the solid and  $N-r+1$  in the liquid. Node number  $r$  is common between the solid and liquid. The solid/liquid interface was considered at nod number  $r$ . Based on the preliminary calculations; the accuracy is acceptable for 50 nodes in the solid and 10 nodes in the liquid.

The main assumptions were made to solve the equations are:

1. Mass transfer is controlled by diffusion alone (convection in the liquid is neglected).
2. The dendrites were considered to have a plate-like morphology.
3. The solid/liquid interface is considered to be at local equilibrium so the composition of solid and liquid at the interface can be extracted from the phase diagram.
4. The whole volume element is at uniform temperature (as the heat transfer is several times faster than the mass transfer, so the temperature gradient in the volume element

is neglected) [20].

5. There is no mass transfer between the volume element and its surroundings. The flux of alloying element at  $x=0$  and  $x=d$  is zero and the equation (7) should be fulfilled.

$$\left( \frac{\partial C_s}{\partial x} \right)_{x=0} = \left( \frac{\partial C_L}{\partial x} \right)_{x=d} = 0 \quad (7)$$

For this purpose the compositions of the nodes number 1 and  $N$  were considered to be equal to the compositions of the nodes number 2 and  $N-1$ , respectively.

According to assumptions number 3 and 5 the required boundary conditions for each phase are based on equations (8-11).

$$(C_s)_1^t = (C_s)_2^t \quad (8)$$

$$(C_s)_r^t = (C_s)_{Eq}^t \quad (9)$$

$$(C_L)_r^t = (C_L)_{Eq}^t \quad (10)$$

$$(C_L)_N^t = (C_L)_{N-1}^t \quad (11)$$

So the equations (8-11) were solved for nodes number 2 to  $r-1$  in solid and  $r+1$  to  $N-1$  in the liquid.

### 3. RESULTS AND DISCUSSIONS

Some examples of cooling curves for 10MgM series are shown in Fig. 2. The cooling curves are smooth and reproducible. Quenching temperatures are indicated by arrows. The DTA curves of the samples quenched after complete solidification can be seen in Fig. 3. The data which are extracted from DTA is presented in Table 2. In this table,  $R$ ,  $T_w$ ,  $T_E$ ,  $\Delta T_w$  and  $t_s$  are cooling rate, solidification start temperature of primary phase ( $\alpha_{A1}$ ), eutectic start temperature,

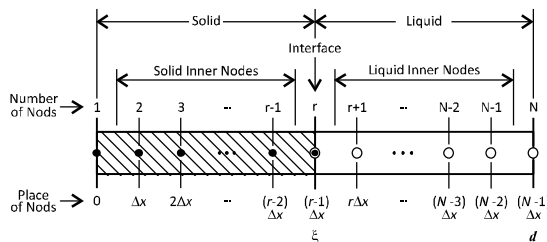


Fig. 1. Schematic of the volume element used for the numerical modelling.

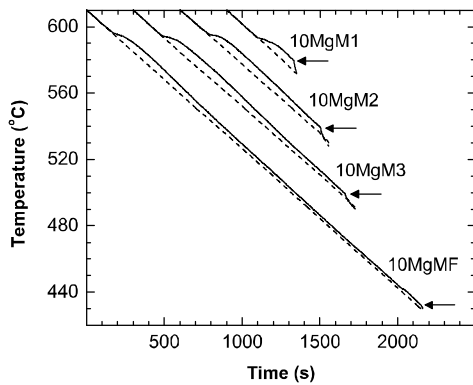


Fig. 2. Cooling curves of the 10MgM series.

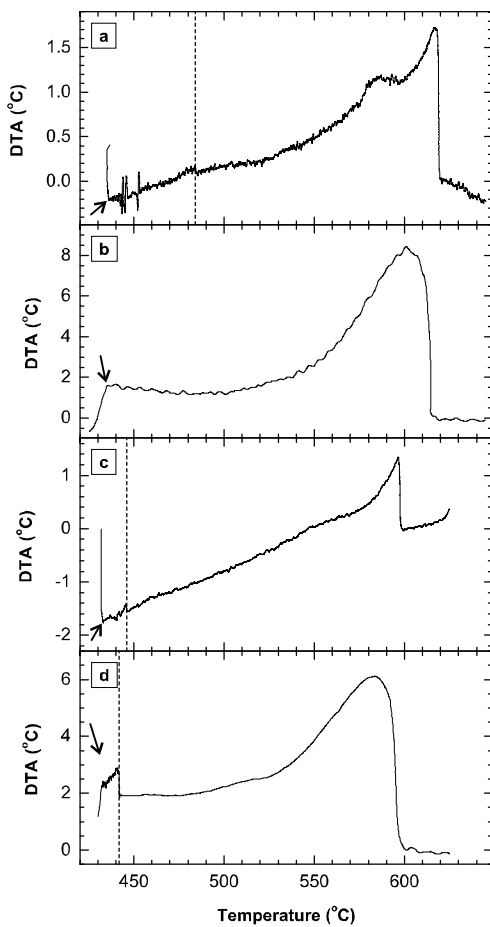


Fig. 3. DTA curves of (a) 7MgSF, (b) 7MgMF, (c) 10MgSF, and (d) 10MgMF.

primary undercooling, and local solidification time, respectively.  $R$ ,  $T_\alpha$ ,  $T_E$ , and  $t_s$  are directly measured from the cooling curve.  $\Delta T_\alpha$  is the difference between the equilibrium liquidus temperature ( $T_{E_L}$ ) from the phase diagram and  $T_\alpha$  ( $\Delta T_\alpha = T_{E_L} - T_\alpha$ ). The parameter  $t_s$  is the time between the start of solidification of  $\alpha_{Al}$  phase (the time which corresponds to the  $T_\alpha$  in the cooling curve) and the end of eutectic reaction. For the sample 7MgMF the eutectic reaction temperature couldn't be determined by the thermal analysis so it was assumed that the  $T_E$  is equal to 10MgMF.

Two peaks can be seen in the DTA curve of 7 MgS which are started at 619.5 and 484 °C, respectively. These peaks are due to the starting and end of the solidification of  $\alpha$ -Al phase so it can be concluded that the alloy should be solidified as single phase alloy. In 7MgM DTA curve, however, just one peak can be seen which starts at 614.5 °C. For 10Mg series two peaks can be seen in both cooling rates. At 0.5 K/min, first peak starts at 598.5 °C for start of solidification of  $\alpha$ -Al phase in 10MgSF and the second one starts at 446 °C for the eutectic reaction. With increasing the cooling rate both peaks are appeared at lower temperatures at 595 and 442 °C for starting of solidification of  $\alpha$ -Al and eutectic reaction, respectively.

Shapes of the DTA curves are somehow different in 0.5 and 5 K/min. In 0.5 K/min curves, the peaks for the beginning of the solidification are sharp. It may be related to the difference in cooling rates. In 7MgSF curve, a very broad peak can be seen after the beginning of the solidification at around 600-570 °C which also has seen in other samples in this series. It seems that this peak does not correspond to any transformation in the sample and it should be a

Table 2. Results of thermal analysis

Alloy Code	$R$ (K/min)	$T_\alpha$ (°C)	$T_E$ (°C)	$\Delta T_\alpha$ (°C)	$t_s$ (s)
7Mg	0.5	619.5	484	1.6	16260
	5	614.5	-	5.4	2183
10Mg	0.5	598.5	446	2.3	18120
	5	595	442	5.3	1883

thermal feature of this alloy in this cooling rate. This will be discussed later in the microstructural analysis section.

Results of  $k_0$  analysis are presented in Table 3. Based on this table, most of the experimental results are much higher than the equilibrium values. Different trends can be seen for  $k_0$  values with temperature in different measurement methods. In Method 1, at 0.5 K/min, the  $k_0$  value increases evenly with decreasing temperature, but at 5 K/min, it decreases first and then increases. In Method 2, with decreasing the temperature, the  $k_0$  value decreases monotonically. In methods 3 and 4 with decreasing the temperature, the  $k_0$  value increases consistently.

It seems that the first two methods show more scatter in trend and values, so it was decided to just use the results of methods 3 and 4 as experimental values. It was also observed that methods 1 and 2 are very sensitive to the experimental input data ( $C_L$  and  $f_L$ ) and to have reliable results the input data should be determined precisely which cannot be achieved

with the current method especially for quenching from high temperatures. Because fraction of the melt in these samples is very high and there will be extensive dilution with the surrounding melt. Especially, there is a possibility for moving of primary phases during quenching which also increases the level of dilution. So, the measured value for  $C_L$  could be less than the exact value and hence the value of  $k_0$  is overestimated.  $f_L$  should also be measured locally and surrounding melt should not be included in the calculations, but the boundary cannot be determined precisely, so the measured value for  $f_L$  will be erroneous. For the method which is based on the lever rule, there is another complexity because of the relation between the results and the phase diagram. To get better results by this method it is necessary to establish the non-equilibrium phase diagram first. In Methods 3 and 4, the  $k_0$  values are calculated based on the composition of the solid which is not affected by quenching process. In these two methods the values agree very well and the trend is the same as the equilibrium trend but the values are noticeably higher than the

**Table 3.** experimental values for  $k_0$  in comparison with the Eq.  $k_0$

Sample code	Experimental $k_0$ by method No.				Eq. $k_0$	Extra. $k_0$
	M1	M2	M3	M4		
7MgS1	0.39	0.30	0.44	-	0.30	-
7MgS2	0.40	0.24	0.55	-	0.33	-
7MgS3	0.53	0.24	0.71	0.55	0.37	-
7MgSF	-	-	0.79	0.67	0.48	0.69
7MgM1	0.47	0.36	0.40	-	0.30	-
7MgM2	0.31	0.18	0.50	-	0.33	-
7MgM3	0.43	0.21	0.56	0.55	0.37	-
7MgMF	-	-	0.67	0.59	0.48	0.58
10MgS1	0.43	0.35	0.43	-	0.33	-
10MgS2	0.46	0.30	0.53	-	0.37	-
10MgS3	0.52	0.29	0.67	0.58	0.41	-
10MgSF	-	-	0.70	0.66	0.48	0.69
10MgM1	0.42	0.34	0.40	-	0.33	-
10MgM2	0.39	0.26	0.45	-	0.37	-
10MgM3	0.48	0.26	0.52	0.45	0.41	-
10MgMF	-	-	0.59	0.57	0.48	0.58

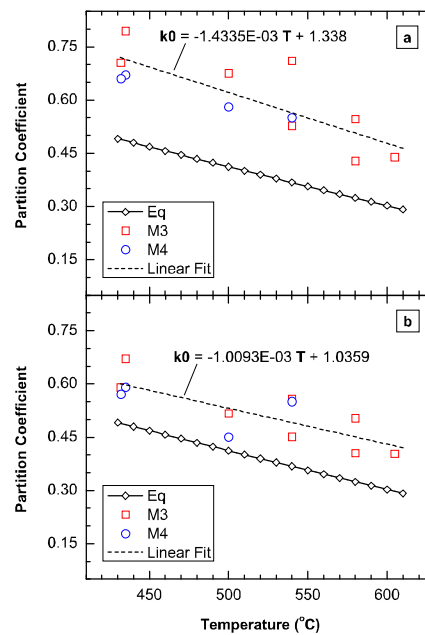


**Fig. 4.** Analysis of partition coefficient for (a) 0.5 and (b) 5 K/min.

equilibrium values. The  $k_0$  value from the methods 3 and 4 with the equilibrium values from phase diagram are shown in Fig. 4.

As can be seen from the equilibrium data presented in Fig. 4, the equilibrium partition coefficient changes linearly with temperature. So it's reasonable to fit a line to the experimental data to have the value of experimental partition coefficient for each cooling rate at any composition and temperature. The fitted lines are also included in Fig. 4. The data from quenched samples were used to fit the curves (dashed line in Fig. 4). Then the lines were extrapolated to predict the  $k_0$  value for the samples quenched after complete solidification. These fitted lines were used to model the microsegregation.

The microstructure of the quenched samples in 7Mg series is shown in Fig. 5. The results of quantitative metallography are presented in Table 4. According to Fig. 5, in both cooling rates, there are just two microstructure constituents in all temperatures, i.e. primary phase and quenched melt. The same trend was seen in 10Mg series.

microstructural (Fig. 5) analyses, the evolution of the microstructure in the samples can be described as below. As the melt temperature reaches to liquidus temperature, the primary phase nucleates. Fraction of solid (primary phase) increases continuously until the end of solidification. If the composition of melt reaches to the eutectic composition, eutectic transformation occurs (e.g. 10Mg in both cooling rates) otherwise it will solidify as a single phase alloy, as in the case of 7Mg at both cooling rates. Based on these results, the broad peak which was seen in DTA curve of 7MgSF, as mentioned before, should be a thermal feature of this alloy in this cooling rate. The origin of the broad peak is not clear to the authors. Each peak in a DTA curve corresponds to a transformation in the sample. As the samples quenched at temperatures lower than the temperature range of this peak (7MgS2 and 7MgS3) show the same microstructural constituents as 7MgS1, so the broad peak does not correspond to any transformation in the sample. Moreover, it cannot be seen in 7MgM series or in 10 Mg alloy samples. Therefore, 7Mg series samples solidify

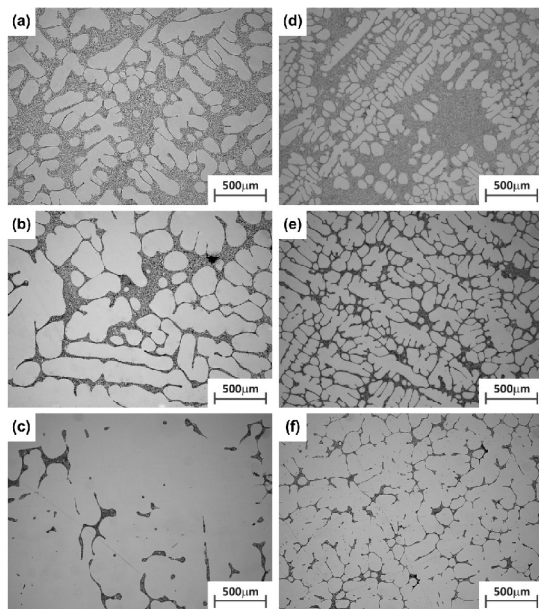


**Fig. 5.** Microstructure of quenched samples of 7Mg alloy, (a) 7MgS1, (b) 7MgS2, (c) 7MgS3, (d) 7MgM1, (e) 7MgM2, and (f) 7MgM3.

**Table 4.** Results of quantitative metallography and SEM/EDS analysis

Sample Code	$f_a^*$ (wt-%)	SDAS ( $\mu\text{m}$ )	$C_{min}$ (wt-%)
7MgS1	55.8	93.2	2.94
7MgS2	76.4	143.2	3.66
7MgS3	92.3	170.4	4.76
7MgSF	100	240.0	5.32
7MgM1	59.8	51.5	2.70
7MgM2	75.8	68.6	3.37
7MgM3	87.3	95.9	3.73
7MgMF	100	101.5	4.49
10MgS1	48.6	99.2	4.36
10MgS2	73.3	139.8	5.38
10MgS3	86.0	170.4	6.88
10MgSF	98.5	200.0	7.19
10MgM1	47.2	48.8	4.13
10MgM2	70.8	65.2	4.60
10MgM3	85.6	74.2	5.27
10MgMF	97.8	78.7	6.02

According to the results of thermal (Fig. 3) and

as single phase alloy at both cooling rates and

there is no eutectic constituent in the microstructure. However, the microstructure of 10Mg samples, as can be seen in Fig. 6, is consisted of primary  $\alpha$ -Al phase and the Mg rich second phase. Some shrinkage pores can also be seen in their microstructure.

Based on the Fig. 5 and Table 4, the microstructure becomes finer with increasing cooling rate and Mg content. In 0.5 K/min, the dendrites are coarse and somewhat globular, but with increasing the cooling rate to 5 K/min their sizes severely decrease and the branching frequency increases.

In Fig. 7, experimental solid fractions are compared with the calculated solidification curves based on the numerical method and the well-known Lever rule and Scheil equation. In order to use Lever rule and Scheil equation, CL was extracted from phase diagram and partition coefficient was assumed to be constant and equal to 0.47. In most cases Lever rule and Scheil equation cannot estimate the solidification path very accurately. It is because of non-realistic assumptions of infinite and zero diffusion

coefficients in the solid for Lever rule and Scheil equation, respectively. They just show the upper and lower boundaries for solidification curves. As can be seen from Fig. 7, except for the highest quenching temperature, experimental solid fractions for all samples lie in this range. The solidification curves which are calculated by numerical method agree very well the experimental results, especially at medium to low temperatures.

The results of secondary dendrite arm spacing (SDAS) measurement are presented in Table 4. It can be seen that by increasing the cooling rate and Mg content, SDAS decreases. Equation (12) was used to estimate SDAS [28].

$$\lambda = k \times t^{0.33} \times C_0^m \quad (12)$$

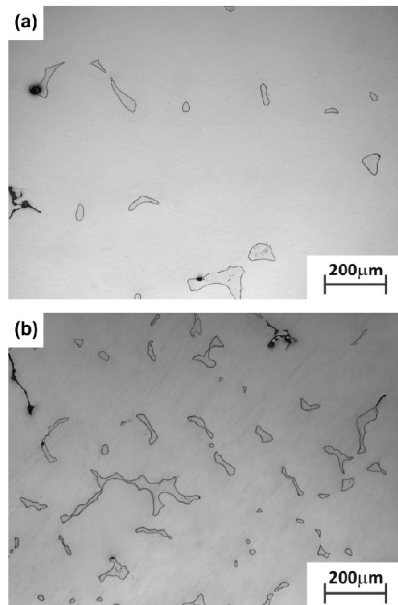


Fig. 6. Microstructure of (a) 10Mg SF, (b) 10Mg MF.

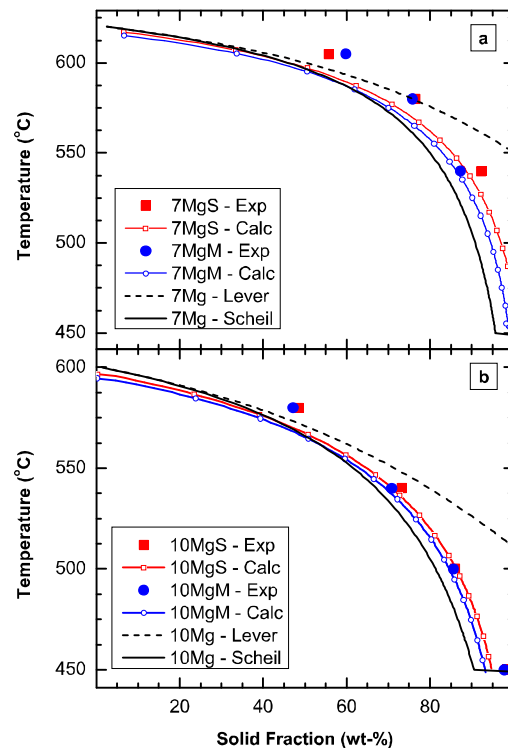


Fig. 7. Experimental solid fraction in comparison with the results of calculation based on the Lever rule, Scheil equation, and the numerical modelling for (a) 7Mg, (b) 10Mg.



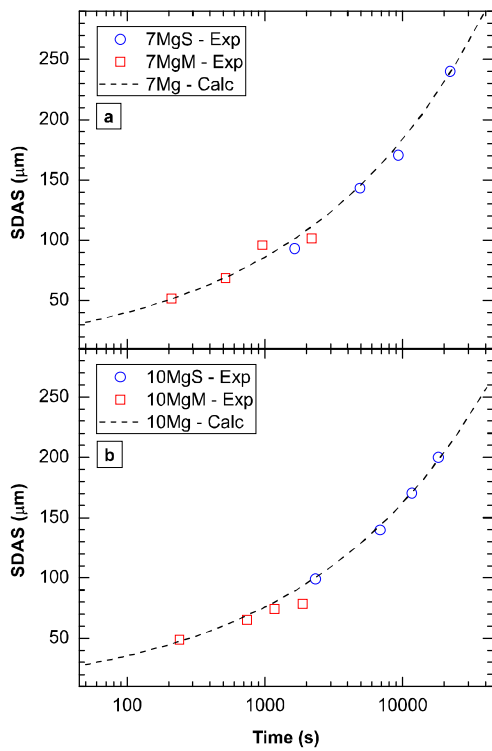


Fig. 8. Experimental results of SDAS in comparison with the calculated results for (a) 7Mg and (b) 10Mg alloys.

where  $\lambda$ ,  $C_0$ , and  $t$  are SDAS, nominal composition, and time.  $k$  is coarsening constant and along with  $m$  can be considered as adjustable parameters which should be determined according to experimental data. In the present study  $k$  and  $m$  are calculated by least square method to be 16.9 and 0.32, respectively. The experimental results and the results of the calculation of SDAS based on the equation (12) are shown in Fig. 8. It can be seen that the experimental results can be accurately estimated by equation (12).

#### 4. SEM/EDX Analysis

Experimental concentration profiles are shown

in Fig. 9. In this figure two other curves based on the Lever rule and Scheil equation are also plotted for comparison. These lines were plotted by assuming  $k_0$  is constant and equal to 0.47. Based on Fig. 9, all experimental profiles deviate from Scheil equation curve. For both 7Mg and 10Mg alloys, by increasing cooling rates from 0.5 to 5 K/min, the beginning of the profiles reduce to lower and their end increase to higher concentrations. With increasing the Mg content, profiles shift to higher concentrations.

Results of numerical modelling are shown in Fig. 10. Two sets of data were used for numerical modelling; equilibrium (EqPD) and experimental (SEPD) data. In EqPD all thermodynamic data were extracted from equilibrium phase diagram. In SEPD CL was extracted from the equilibrium phase diagram and experimental partition coefficient was used to calculate the CS by using equation (1). It seems that the results of SEPD

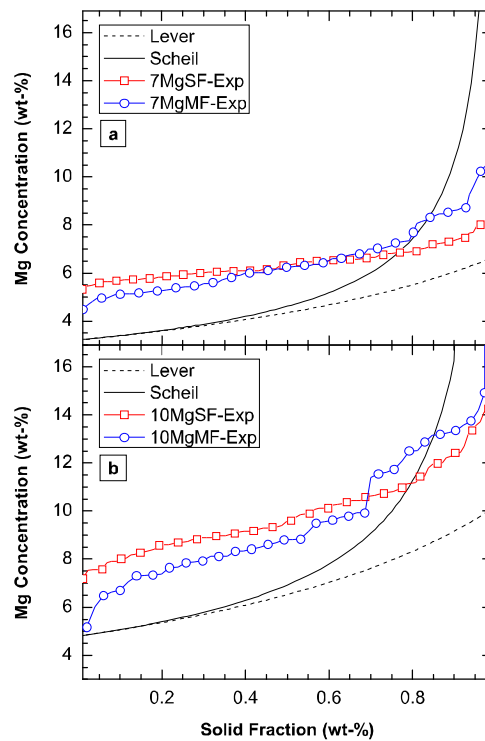


Fig. 9. Experimental concentration profiles of (a) 7Mg and (b) 10Mg alloy.

calculations show better correlation with

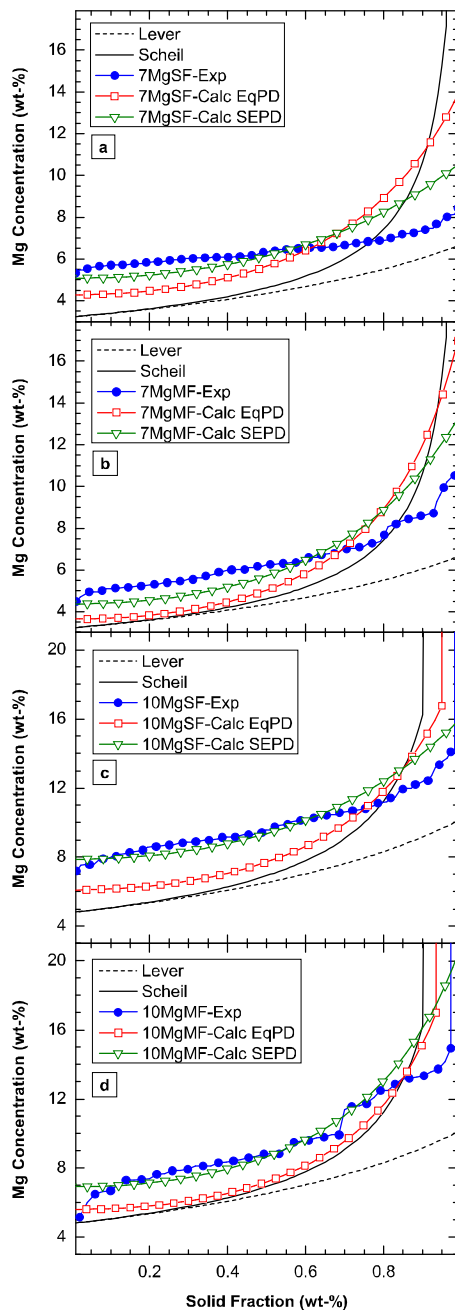


Fig. 10. Calculated profiles in comparison with the experimental profiles for (a) 7MgSF, (b) 7MgMF, (c) 10MgSF, and (d) 10MgMF.

experimental profiles than the EqPD calculations.

## 5. CONCLUSION

In the current study, partition coefficient was experimentally analyzed for binary Al-Mg alloys and the results were validated by numerical modeling. Four methods were used to calculate the partition coefficient. It seems the methods which are based on the concentration of the solid (minimum concentration or concentration profile in the primary phase) are more consistent and reliable. The results of modeling using these data show better correlation with experimental results.

## 6. ACKNOWLEDGMENT

The technical support by “Royal Institute of Technology” (KTH) is appreciated. M. H. Avazkonandeh-Gharavol appreciates the financial support by Ministry of Sciences, Research and Technology of Islamic Republic of Iran during his visit to the KTH. Haji M. Muhmond and S. Salim are gratefully acknowledged for help to set up the experiments.

## REFERENCES

1. Fornaro, O. and Palacio, H. A., “Study of dilute Al-Cu solidification by cooling curve analysis”. *J. Mater. Sci.*, 2009, 44, 4342-4347.
2. Dong, H. B., Shin, M. R. M., Kurum, E. C., Cama, H. and Hunt, J. D., “Determination of liquid fraction during solidification of aluminium alloys using a single-pan scanning calorimeter”. *Fluid Phase Equilib.*, 2003, 212, 199-208.
3. Larouche, D., Laroche, C. and Bouchard, M., “Analysis of differential scanning calorimetric measurements performed on a binary aluminium alloy”. *Acta Mater.*, 2003, 51, 2161-2170.
4. Polmear, I. J., “Light Alloys”. From Traditional Alloys to Nanocrystals, MA, USA, 2006, 227-228.
5. Roosz, A., Halder, E. and Exner, H. E., “Numerical calculation of microsegregation in coarsened dendritic microstructures”. *Mater. Sci. Technol.*, 1986, 2, 1149-1155.
6. Voller, V. R. and Sundarraj, S., “Modeling of micro-segregation”. *Mater. Sci. Technol.*, 1993, 9, 474-482.
7. Kraft, T., Rettenmayr, M. and Exner, H. E., “An

- extended numerical procedure for predicting microstructure and microsegregation of multicomponent alloys”. *Modell. Simul. Mater. Sci. Eng.*, 1996, 4, 161-177.
8. Turkeli, A., “Approximate analytical models for micro-segregation considering the effect of dendrite arm coarsening”. *Mater. Sci. Forum*, 2006, 508, 449-454.
  9. Du, Q. and Jacot, A., “A two-dimensional micro-segregation model for the description of microstructure formation during solidification in multicomponent alloys: Formulation and behaviour of the model”. *Acta Mater.*, 2005, 53, 3479-3493.
  10. Battle, T. P., “Mathematical modelling of solute segregation in solidifying materials”. *Int. Mater*, 1992, 37, 249-270.
  11. Fredriksson, H. and Akerlind, U., “Solidification and crystallization processing in metals and alloys”, London, 2012, pp. 71-75.
  12. Yan, X., Xie, F., Chu, M. and Chang, Y. A., “Micro-segregation in Al-4.5Cu wt.% alloy: experimental investigation and numerical modeling”. *Mater. Sci. Eng. A*, 2001, 302, 268-274.
  13. Liang, H., Kraft, T. and Chang, Y. A., “Importance of reliable phase equilibria in studying microsegregation in alloys: Al-Cu-Mg”. *Mater. Sci. Eng. A*, 2000, 292, 96-103.
  14. Kurum, E. C., Dong, H. B. and Hunt, J. D., “Micro-segregation in Al-Cu alloys”. *Metall. Mater. Trans. A*, 2005, 36, 3103-3110.
  15. Chen, S. W. and Huang, C. C., “Solidification curves of Al-Cu, Al-Mg and Al-Cu-Mg alloys”. *Acta mater.*, 1996, 44, 1955-1965.
  16. Liu, Y. L. and Kang, S. B., “Solidification and segregation of Al-Mg alloys and influence of alloy composition and cooling rate”. *Mater. Sci. Technol.*, 1997, 13, 331-336.
  17. Gungor, M. N., “A statistically significant experimental technique for investigating microsegregation in cast alloys”. *Metall. Trans. A*, 1989, 20, 2529-2533.
  18. Valdes, J., Shang, S. L., Liu, Z. K., King, P. and Liu, X., “Quenching differential thermal analysis and thermodynamic calculation to determine partition coefficients of solute elements in simplified Ni-base superalloys. *Metall*”. *Mater. Trans. A*, 2010, 41, 487-498.
  19. Kraft, T. and Chang, Y. A., “Discussion of Effect of Dendrite Arm Coarsening on Microsegregation. *Metall*”. *Mater. Trans. A*, 1998, 29, 2447-2449.
  20. Sundarraj, S. and Voller, V. R., “The binary alloy problem in an expanding domain: the microsegregation problem”. *Int. J. Heat Mass Transfer*, 1993, 36, 713-723.
  21. Tanzilli, R. A. and Heckel, R.W., “Numerical solutions to the finite, diffusion-controlled, two-phase, moving-interface problem (with planar, cylindrical, and spherical interfaces)”. *Trans. AIME*, 1968, 242, 2312-2321.